Attosecond-magnetic-field-pulse generation by intense few-cycle circularly polarized UV laser pulses

Kai-Jun Yuan and André D. Bandrauk[*]

Département de Chimie, Faculté des Sciences, Université de Sherbrooke, Sherbrooke, Québec, Canada, J1K 2R1
(Received 2 March 2013; revised manuscript received 6 July 2013; published 23 July 2013)

Intense attosecond-magnetic-field pulses are predicted to be produced by intense few-cycle attosecond circularly polarized UV pulses. Numerical solutions of the time-dependent Schrödinger equation for H_2^+ are used to study the electronic dynamical process. Spinning attosecond circular electron wave packets are created on subnanometer molecular dimensions, thus generating attosecond magnetic fields of several tens of Teslas (10^5 G). Simulations show that the induced magnetic field is critically dependent on the pulse wavelength λ and pulse duration $n\tau$ (n is number of cycles) as predicted by a classical model. For ultrashort few-cycle circularly polarized attosecond pulses, molecular orientation influences the generation of the induced magnetic fields as a result of preferential ionization perpendicular to the molecular axis. The nonspherical asymmetry of molecules allows for efficient attosecond-magnetic-field-pulse generation.

PACS number(s): 33.20.Xx, 33.90.+h

I. INTRODUCTION

The rapid developments in synthesizing ultrashort intense pulses offer the possibility to investigate electron dynamics on its natural time scale, the attosecond (1 as $= 10^{-18}$ s) in the nonlinear nonperturbative regime of laser molecule interaction [1–3]. To date, the shortest linearly polarized single pulse with a duration of 67 as has been produced from high-order harmonic generation (HHG) with a few-cycle intense infrared laser field in atoms [4]. With a midinfrared femtosecond laser HHG spectra of very high order ∼5000 (1.6 keV) can also be generated, thus allowing for the generation of pulses as short as a few attoseconds [5]. With such attosecond pulses electrons in matter can then be visualized and controlled on the attosecond time scale and subnanometer dimension, e.g., [6–9]. An application of such pulses is the monitoring of coherent superposition of two or more bound electronic states in atomic or molecular systems, which lead to electron motion on an attosecond time scale with momentum distributions [10] or HHG spectra [11] measurable as a function of the time delay between pump-probe pulses. However, the development of attosecond pulse technology has been limited to linear polarization. Circularly polarized attosecond pulses have now been proposed as future tools for studying further attosecond electron dynamics [12–15]. We have previously proposed methods of generating such circularly polarized attosecond pulses from circularly polarized molecular HHG due to the nonsymmetry of molecular Coulomb potentials [16]. Atomic Coulomb potentials can also control recollision of electrons in double ionization with circular polarization for specific atomic parameters [13].

Optically induced ultrafast magnetization reversal has now been reported by circularly polarized pulses in material science [14], thus emphasizing new and future application of such pulses. Optically induced magnetic fields have been previously related to the inverse Faraday effect [17], for which a perturbative weak magnetic field treatment has been presented in terms of optical polarizabilities [18]. Recently, the generation of electronic ring currents in aromatic molecules obtained from quantum-chemical numerical simulations can produce static magnetic fields by means of linearly [19] and circularly polarized π UV pulses resonant with degenerate π orbitals [20,21]. The generated magnetic fields can be much larger than those obtained by traditional static fields [22]. The driving pulses can be optimized as well by optimal control theory [23]. In these previous studies, coherent rotational electronic states are prepared resonantly, thus leading to static magnetic fields. Moreover, these induced effects strongly rely on the coherence of the excited states. With intense circularly polarized attosecond pulses, we have proposed to create "spinning" continuum electrons which can be produced and localized on the subnanometer molecular dimensional scale [24]. As a result, circular electron wave packets and currents are created in the continuum and thus large internal molecular magnetic fields are generated. In this paper we show that intense attosecond-magnetic-field pulses can be obtained from intense few-cycle circularly polarized attosecond UV pulses, as illustrated in Fig. 1. The developments of circularly polarized attosecond pulses [16] thus make it possible to create spinning circular electron wave packets, leading to large time-dependent internal magnetic fields in matter on the attosecond time scale.

The paper is arranged as follows: In Sec. II we briefly describe the computational methods for time-dependent quantum electron wave packets for calculations from the corresponding TDSEs. The numerical results of time-dependent electronic currents and magnetic fields by intense ultrashort few-cycle circularly polarized UV pulses for H_2^+ are presented in Sec. III. Effects of the pulse wavelength and molecular orientation are also presented. Finally, we summarize our findings in Sec. IV. Throughout this paper, atomic units (a.u.) $e = \hbar = m_e = 1$ are used unless otherwise stated.

II. NUMERICAL METHODS

Simulations are performed on an oriented fixed nuclei molecular ion H_2^+ from numerical solutions of the corresponding time-dependent Schrödinger equation (TDSE) within a static (Born-Oppenheimer approximation, BOA) nuclear

*andre.bandrauk@usherbrooke.ca
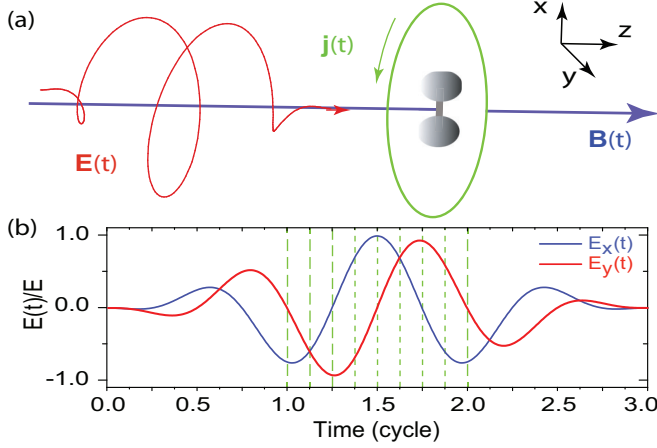
FIG. 1. (Color online) (a) Illustration of the attosecond magnetic fields $\mathbf{B}(\mathbf{r},t)$ (blue line, along the z axis) for H_2^+ by a few-cycle circularly polarized attosecond UV pulse (red line). The green line represents the corresponding current $\mathbf{j}(\mathbf{r},t)$ in the molecular (x,y) plane. The magnetic field $\mathbf{B}(\mathbf{r},t)$ is perpendicular to the current $\mathbf{j}(\mathbf{r},t)$. (b) Three-cycle circularly polarized attosecond UV pulse $\mathbf{E}(t)$ at $\lambda = 50$ nm. Dashed lines correspond to the times in Figs. 2 and 3, and Table I.

frame,

$$i\frac{\partial}{\partial t}\psi(\mathbf{r},t) = [\hat{H}_0 + V_L(\mathbf{r})]\psi(\mathbf{r},t), \qquad (1)$$

where H_0 is the field-free molecular Hamiltonian and $V_L(\mathbf{r})$ is the interaction term. Such a fixed nuclei approach by ignoring the vibrational and rotational degrees of freedom is appropriate due to the longer femtosecond or picosecond time scale of nuclear (vibrational or rotational) motions. The corresponding three-dimensional (3D) TDSE is solved using cylindrical coordinates $\mathbf{r} = (\rho,\theta,z)$ with the molecular plane $x = \rho\cos\theta$ and $y = \rho\sin\theta$ [Fig. 1(a)]. The molecular Hamiltonian is expressed as

$$H_0(\rho,\theta,z) = -\frac{1}{2\rho}\frac{\partial}{\partial\rho}\left(\rho\frac{\partial}{\partial\rho}\right) - \frac{1}{2\rho^2}\frac{\partial^2}{\partial\theta^2}$$
$$- \frac{1}{2}\frac{\partial^2}{\partial z^2} + V(\rho,\theta,z), \qquad (2)$$

where $V(\rho,\theta,z)$ is the two center electron-nuclear potential. The molecular ion is preoriented before ionization and this can be readily achieved with orientational laser technology [25]. The radiative interaction between the laser field and the electron is described by

$$V_L(\mathbf{r}) = \mathbf{r}\cdot\mathbf{E}(t) = \hat{e}_x\rho\cos\theta E_x(t) + \hat{e}_y\rho\sin\theta E_y(t) \qquad (3)$$

in the length gauge for circularly polarized pulses, $\mathbf{E}(t) = Ef(t)[\hat{e}_x\cos(\omega t) + \hat{e}_y\sin(\omega t)]$, propagating in the z direction, and $\hat{e}_{x/y}$ is the polarization direction. A smooth $\sin^2(\pi t/n\tau)$ pulse envelope $f(t)$ for maximum amplitude E and intensity $I = I_x + I_y = c\varepsilon_0 E^2$ is adopted, where one optical cycle $\tau = 2\pi/\omega$. This pulse satisfies the total zero area $\int E(t)dt = 0$ in order to exclude static field effects [26,27].

The 3D TDSE in Eq. (1) is solved numerically by a second-order split operator method [26] in the time step δt combined with a fifth-order finite difference method and

Fourier transform technique in the spatial steps $\delta\rho$, δz, and $\delta\theta$ [27]. The time step is taken to be $\delta t = 0.01$ a.u. $= 0.24$ as. The spatial discretization is $\delta\rho = \delta z = 0.25$ a.u. for a radial grid range $0 \leqslant \rho \leqslant 128$ a.u. (6.77 nm) and $|z| \leqslant 32$ a.u. (1.69 nm), and the angle grid size $\delta\theta = 0.025$ rad. To prevent unphysical effects due to the reflection of the wave packet from the boundary, we multiply $\psi(\rho,\theta,z,t)$ by a "mask function" or absorber in the radial coordinates ρ with the form $\cos^{1/8}[\pi(\rho - \rho_a)/2\rho_{abs}]$. For all results reported here we set the absorber domain $\rho_a = \rho_{max} - \rho_{abs} = 104$ a.u. with $\rho_{abs} = 24$ a.u., exceeding well the field induced electron oscillation $\alpha_d = E/\omega^2$ of the electron.

The time-dependent electronic current density is defined by the quantum expression

$$\mathbf{j}(\mathbf{r},t) = \frac{i}{2}[\psi(\mathbf{r},t)\nabla_\mathbf{r}\psi^*(\mathbf{r},t) - \psi^*(\mathbf{r},t)\nabla_\mathbf{r}\psi(\mathbf{r},t)], \qquad (4)$$

$\psi(\mathbf{r},t)$ is the exact BOA electron wave function obtained from the TDSE and $\nabla_\mathbf{r} = \mathbf{e}_\rho\nabla_\rho + \mathbf{e}_\theta\frac{1}{\rho}\nabla_\theta + \mathbf{e}_z\nabla_z$ in cylindrical coordinates. Then the corresponding time-dependent magnetic field is calculated using the following classical Jefimenko's equation [28]:

$$\mathbf{B}(\mathbf{r},t) = \frac{\mu_0}{4\pi}\int\left[\frac{\mathbf{j}(\mathbf{r}',t_r)}{|\mathbf{r} - \mathbf{r}'|^3} + \frac{1}{|\mathbf{r} - \mathbf{r}'|^2 c}\frac{\partial\mathbf{j}(\mathbf{r}',t_r)}{\partial t}\right]$$
$$\times (\mathbf{r} - \mathbf{r}')d^3\mathbf{r}', \qquad (5)$$

where $t_r = t - r/c$ is the retarded time and $\mu_0 = 4\pi \times 10^{-7}$ N A^{-2} (6.692×10^{-4} a.u.). Units of $B(\mathbf{r},t)$ are Teslas (1 T = 10^4 G). For the static time-independent conditions occurring after the pulse, then Eq. (5) reduces to the classical Biot-Savart law [28].

III. RESULTS AND DISCUSSIONS

In the present simulations, the molecule is initially in the ground $1s\sigma_g$ state of H_2^+ at equilibrium $R_e = 2$ a.u. with the ionization potential $I_p = 1.1$ a.u. (29.72 eV). The initial corresponding wave function $\psi(\mathbf{r},t = 0)$ is obtained by propagating an initial appropriate wave function in imaginary time using the zero-field TDSE [26,27]. We adopt a circularly polarized attosecond UV pulse with intensity $I = 2 \times 10^{16}$ W/cm^2 ($E = 0.5338$ a.u.), corresponding to $I_x = I_y = 1 \times 10^{16}$ W/cm^2, wavelength $\lambda = 50$ nm ($\omega = 0.911$ a.u.), and duration $3\tau = 500$ as. With such pulses of broad spectral width ~ 0.44 a.u. $= 11.97$ eV, a single photon absorption is possible releasing the electron with near zero initial velocity $v(t_0) \approx 0$. The Keldysh parameter $\gamma = \sqrt{I_p/2U_p} = 2.5$, where $U_p = E^2/4\omega^2$ is the ponderomotive energy, indicates a region of multiphoton ionization processes [30,31].

For the x oriented H_2^+ ionized by circularly polarized attosecond UV pulses propagating along the z axis (Fig. 1), the current densities $|\mathbf{j}(\mathbf{r},t)|$ (fs^{-1}) are mainly localized in the molecular plane (x,y) and the corresponding magnetic fields $\mathbf{B}(\mathbf{r},t)$ (T) are along the z axis, perpendicular to the molecule, as predicted in Eqs. (4) and (5) and illustrated in Fig. 1. We illustrate in Fig. 2 snapshots of the induced attosecond magnetic fields $\mathbf{B}(z,\theta,t)$ averaged over ρ (left column) as a function of angle θ in the (x,y) molecular plane and $\mathbf{B}(z,\rho,t)$ averaged over θ (right column) as a function of
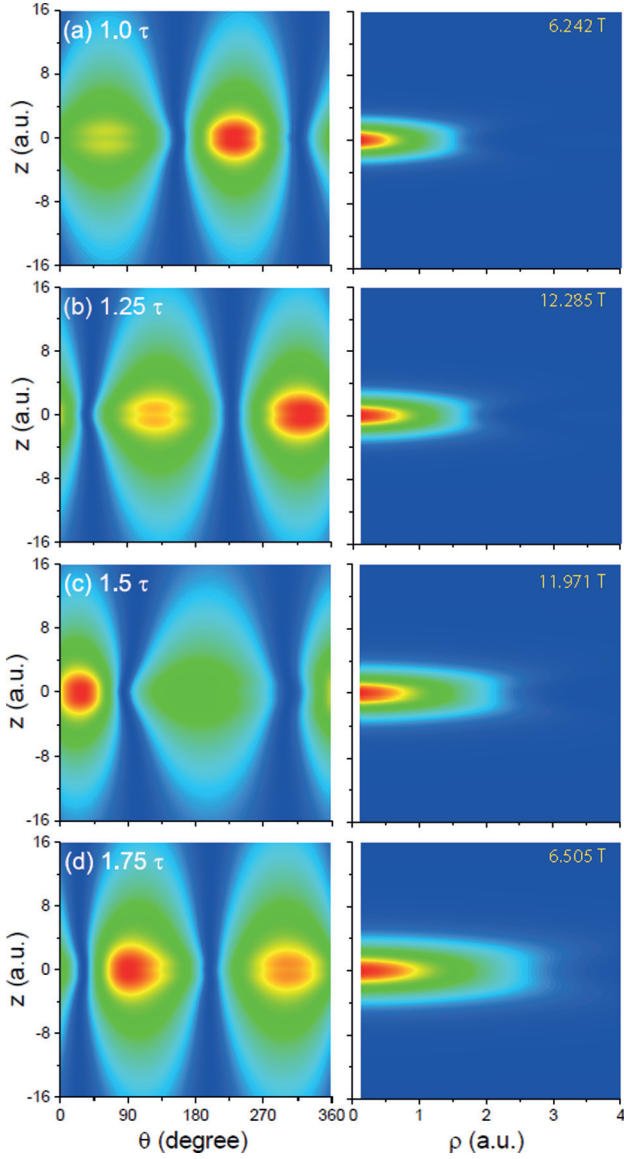
FIG. 2. (Color online) Attosecond magnetic fields $|\mathbf{B}(z,\theta,t)|$ $[\theta = \tan^{-1}(y/x)]$ (left column) and $|\mathbf{B}(z,\rho,t)|$ (right column) at different moments generated by circularly polarized attosecond UV pulses, illustrated in Fig. 1 with intensity $I = 2 \times 10^{16}$ W/cm^2 ($E = 0.5338$ a.u.), wavelength $\lambda = 50$ nm ($\omega = 0.911$ a.u.), and duration $3\tau = 500$ as. The corresponding values of the magnetic field strengths (T) are listed in Table I. The corresponding maximum local magnetic fields $B_{\max}(\mathbf{r},t)$ are, respectively, (a) 6.242 T at $t = 1.0\tau$, (b) 12.285 T at $t = 1.25\tau$, (c) 11.971 T at $t = 1.5\tau$, and (d) 6.505 T at $t = 1.75\tau$.

radial coordinates at different moments around the peak time $t = 1$–2τ of the pulse. The magnetic fields evolve around the z axis in the (x,y) plane due to the circularly polarized pulses. There are two field components which are symmetric with respect to the molecular (x,y) plane and centered at $z \approx \pm 1$ a.u. (0.0529 nm) above and below the molecular plane. The magnetic fields rotate from angles $\theta = -90°$ (270°) to 90° with time, and at $1.25\tau \leqslant t \leqslant 1.5\tau$, the field is maximum at $\theta = 360°$ (0°) parallel to the molecular x or R axis. The corresponding current densities $|\mathbf{j}(x,y,t)|$ obtained by
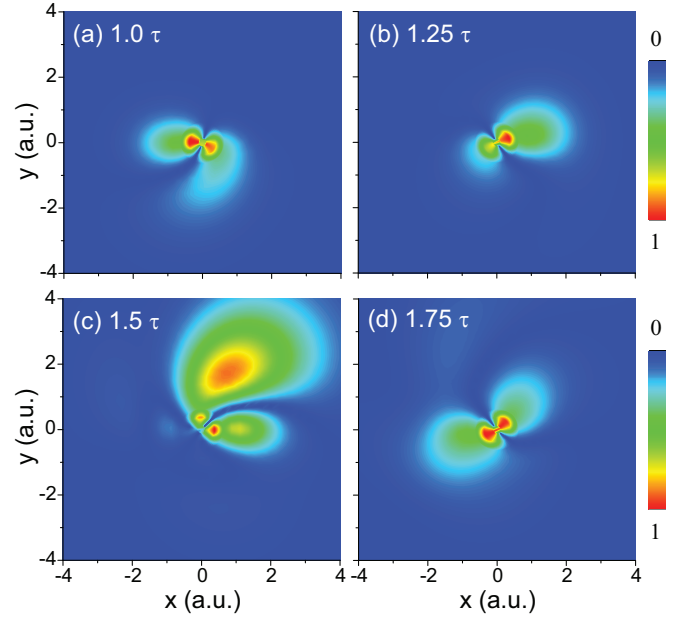
FIG. 3. (Color online) Evolution of current densities $|\mathbf{j}(x,y,t)|$ (fs^{-1} a_0^{-1}) with time t generated by circularly polarized attosecond UV pulses with intensity $I = 2 \times 10^{16}$ W/cm^2, wavelength $\lambda = 50$ nm, and duration $3\tau = 500$ as, corresponding to Fig. 2. The corresponding values of the currents are listed in Table I.

integrating over z perpendicular to the molecular plane are also displayed in Fig. 3. From Figs. 2 and 3 one sees that both $|\mathbf{j}(x,y,t)|$ and $\mathbf{B}(z,\theta,t)$ spirally rotate with an anticlockwise direction, following the left-handed polarization.

For a circularly polarized pulse with wavelength $\lambda = 50$ nm below the ionization threshold and duration $3\tau = 500$ as, the corresponding spectral width at half maximum is about $\Delta\omega = 0.44$ a.u. After absorption of one photon of frequency $\omega = 0.911$ a.u., electron wave packets are created in the continuum with relatively small kinetic energy with dominant distributions near zero initial velocity. The electron wave packets then move under the influence of the intense pulse. As a result, the current appears in the molecular (x,y) plane perpendicular to the propagation z direction. This time-dependent current produces a dynamical attosecond magnetic field which is a function of the pulse phase ωt.

We calculate the maximum local $B_{\max}(\mathbf{r},t)$ and total volume average attosecond magnetic fields and the corresponding currents by integrating $B(t) = |\int \mathbf{B}(\mathbf{r},t)d\mathbf{r}^3|$ and $j(t) = |\int \mathbf{j}(\mathbf{r},t)d\mathbf{r}^3|$ $(d\mathbf{r}^3 = \rho d\rho d\theta dz)$ over the electron $\mathbf{r}$ space. Table I lists values of $B_{\max}(\mathbf{r},t)$, $B(t)$, and $j(t)$ at different moments, illustrated in Figs. 2 and 3. Both $B(t)$ (in units of T a_0^3, where a_0 is Bohr radius) and $j(t)$ (fs^{-1} a_0) vary with time, increasing first and then decreasing in phase with the pulse. In Figs. 2 and 3 we see that the induced volume electronic currents and the attosecond volume magnetic-field pulses are localized and concentrated in space. From Table I one obtains that the maximum total volume magnetic field is induced at $t = 1.625\tau = 270$ as with strength $B = 1.172 \times 10^{-4}$ a.u. $= 29.3$ T a_0^3 (2.93×10^5 G a_0^3). The maximum local magnetic field $B_{\max}(\mathbf{r},t) = 12.285$ T and the maximum electronic current $j = 0.304$ a.u. $= 12.568$ fs^{-1} a_0 (2.011 mA a_0) is produced at time $t = 1.25\tau = 207$ as, where $E_x = 0$ and

TABLE I. Maximum local $B_{max}(\mathbf{r},t)$ and total volume magnetic field $B(t)$ and currents $j(t)$ by circularly polarized attosecond UV pulses with intensity $I = 2 \times 10^{16}$ W/cm^2, wavelength $\lambda = 50$ nm, and duration $3\tau = 500$ as at different times, cf. Figs. 2 and 3.

	Units	1.0τ	1.25τ	1.5τ	1.625τ	1.75τ	2.0τ
$B_{max}(\mathbf{r},t)$	$\times 10^{-4}$ a.u.	0.250	0.491	0.479	0.365	0.260	0.167
	T	6.242	12.285	11.971	9.121	6.505	4.167
$B(t)$	$\times 10^{-4}$ a.u.	0.267	0.705	1.112	1.172	1.101	0.693
	T a_0^3	6.670	17.612	27.797	29.300	27.517	17.320
	a.u.	0.126	0.304	0.257	0.247	0.249	0.202
$j(t)$	fs^{-1} a_0	5.209	12.568	10.625	10.211	10.294	8.351
	mA a_0	0.834	2.011	1.700	1.634	1.674	1.336

$E_y = -E$ (Fig. 1). A time delay $\Delta t = 0.375\tau = 63$ as occurs between maximum current $j(t = 1.25\tau) = 12.568$ fs^{-1} a_0 and $B(t = 1.625\tau) = 29.3$ T a_0^3 (Table I). As shown in Fig. 1, the ionization mainly occurs at $1.125\tau \leqslant t \leqslant 1.25\tau$, where E_y is maximum due to the nonspherical molecular Coulomb potential [29]. Thus the maximum current is obtained as listed in Table I. After ionization, the electron moves following the electric fields $E_x > 0$ and $E_y < 0$, leading the rotation trajectory with anticlockwise direction, as illustrated in Figs. 3(b) and 3(c). At time $t = 1.625\tau$ the maximum total magnetic field is produced. From Fig. 3 one then observes the magnetic field angle is near 90°, corresponding to the y axis, essentially perpendicular to the molecular R axis.

We next show effects of the pulse wavelength λ and pulse duration $n\tau$ on the magnetic field. The maximum values of the local magnetic field strength $\mathbf{B}(\mathbf{r} = 0)$ at $\mathbf{r} = 0$, the center of the molecule is displayed in Fig. 4. We fix the pulse intensity at $I = 2 \times 10^{16}$ W/cm^2. The pulse wavelength is varied from $\lambda = 20$ to 70 nm for different pulse durations $n\tau$, where $n = 3, \ldots, 6$ is the number of cycles. $\mathbf{B}(\mathbf{r} = 0)$ strongly depends on these pulse parameters. At short wavelength $\lambda = 20$ nm weak $|\mathbf{B}(\mathbf{r} = 0)| \approx 0.17$ T are induced, which however are insensitive to the pulse duration $n\tau$. Increasing λ the corresponding magnetic field increases gradually. One sees that the results for the 3τ pulses vary
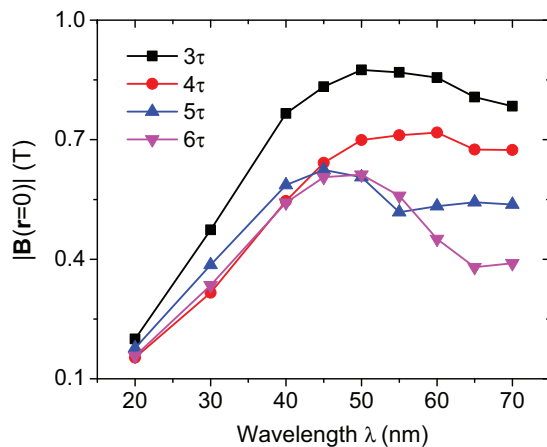
FIG. 4. (Color online) Maximum values of the induced local magnetic fields $|\mathbf{B}(\mathbf{r} = 0)|$ (T) at the central point $\mathbf{r} = 0$ by $I = 2 \times 10^{16}$ W/cm^2 circularly polarized UV laser pulses with different wavelengths λ and durations $n\tau$ (cycles).

quickly. At $\lambda = 50$ nm the magnetic field reaches a maximum strength $|\mathbf{B}(\mathbf{r} = 0)| = 0.88$ T, five times stronger than that at $\lambda = 20$ nm. For the case of $n \geqslant 4$ cycles, the magnetic field is nearly insensitive to the pulses duration. Increasing the pulse wavelength λ or decreasing the frequency ω further, the magnetic field decreases since the induced electron radius is inversely proportional to the frequency ω as described next. Moreover, as the pulse duration $n\tau$ increases $\mathbf{B}(\mathbf{r} = 0)$ decreases dramatically. At $\lambda = 70$ nm, the magnetic field strength of 3τ is twice that of 6τ.

At shorter pulse wavelengths $\omega > I_p$ or higher frequencies, the molecule is ionized after absorption of one photon and the corresponding continuum electron with initial velocity $\sqrt{2(\omega - I_p)}$ moves away from the molecular center directly but mainly perpendicular to the molecular R axis, i.e., the y direction [29] due to a nonzero drift velocity in the y direction [30]. Furthermore, ionization rates are also weak. Weaker magnetic fields are obtained which are nearly insensitive to the pulse duration τ. For the lower pulse frequency $\omega \lesssim I_p$, the electron is released from the molecules with low initial velocities by absorbing one photon due to the broad spectral width of pulses. The electron trajectories are functions of the pulse wavelength λ (frequency ω) and duration $n\tau$ [24]. We explain this from the classical model [24], a generalization of the linear polarization model [31]. Assuming the zero initial electron velocities $\dot{x}(t_0) = \dot{y}(t_0) = 0$, where t_0 is the ionization time, the induced time-dependent velocities are

$$\dot{x}(t) = -E/\omega(\sin \omega t - \sin \omega t_0),$$
$$\dot{y}(t) = -E/\omega(\cos \omega t_0 - \cos \omega t). \tag{6}$$

The corresponding displacements are

$$x(t) = -E/\omega^2[\cos \omega t_0 - \cos \omega t - (\omega t - \omega t_0)\sin \omega t_0],$$
$$y(t) = -E/\omega^2[\sin \omega t_0 - \sin \omega t + (\omega t - \omega t_0)\cos \omega t_0], \tag{7}$$

with $x(t_0) = y(t_0) = 0$ corresponding to recollision at the center of the molecule ($r = 0$). From Eqs. (6) and (7) it is found that increasing the pulse wavelength λ leads to increase of the maximum induced electron velocity $v = 2E/\omega$ at $\omega t - \omega t_0 = (2n' + 1)\pi$, and the corresponding radii

$$r_{n'} = 2E/\omega^2[1 + (n' + 1/2)^2\pi^2]^{1/2}, \tag{8}$$

$n' = 0, 1, 2, \ldots$. For a moving point charge the corresponding classical magnetic field can be expressed as

$$\mathbf{B} = \frac{\mu_0}{4\pi}\frac{\mathbf{v} \times \mathbf{r}}{\mathbf{r}^3}. \tag{9}$$

From Eqs. (6), (7), and (9) one then gets the maximum field $B \sim 1/r_{n'}^2$ at times $t_0 + (2n' + 1)\pi/\omega$. Therefore, an increase of λ or lower ω results in a decrease of the magnetic field due to large radii $r_{n'}$ of the electron, thus reducing the efficiency of the attosecond magnetic field generation. Longer pulse durations have a similar effect. Of note is that we only present the results for the single photon ionization processes. Increasing the pulse wavelength further, more photons are required to ionize molecules, resulting in a decrease of the ionization rate and an increase of the radii of the free photoelectron. Consequently, weaker magnetic-field pulses are produced, see Eq. (9).
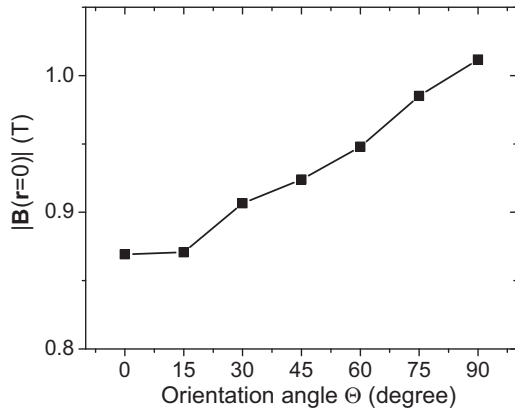
FIG. 5. Maximum values of the laser induced local magnetic fields $|\mathbf{B}(\mathbf{r} = 0)|$ (T) at $\mathbf{r} = 0$ by intense circularly polarized UV laser pulses with intensity $I = 2 \times 10^{16}$, wavelengths $\lambda = 50$ nm, and durations $3\tau = 500$ as for different orientation angles Θ between the molecular R axis and the E_x field component.

For few-cycle circularly polarized attosecond pulses, the molecular orientation can also influence the magnetic field. In Fig. 5 we display the maximum values of the local $|\mathbf{B}(\mathbf{r} = 0)|$ for different angles Θ, where Θ is the molecular orientation angle between the molecular R axis and the x axis, the direction of the E_x component. $|\mathbf{B}(\mathbf{r} = 0)|$ increase as Θ increases. The same pulse is used as in Fig. 2. For the three-cycle circularly polarized attosecond pulse, maxima of the $E_x(t)$ and $E_y(t)$ field components are not equal. Moreover, due to the nonspherical molecular Coulomb potential the ionization ratio between the parallel x and the perpendicular y polarizations is unequal and the ionization probability is dominant perpendicular to the molecular R axis due to two center interference [29] and perpendicular drift [30]. Since the ionization probability is sensitive to Θ, a change of the molecular orientation influences the current as well as the magnetic field. As illustrated in Fig. 1(b) the maximum of the field component $E_x(t = 1.5\tau) = E$ is slightly stronger than that of $E_y(t = 1.25\tau) = 0.93E$ for the molecular ionization. The largest magnetic field is then obtained at $\Theta = 90°$ with $|\mathbf{B}(\mathbf{r} = 0)| = 1.01$ T.

IV. CONCLUSIONS

In summary, we have theoretically presented a generation of intense dynamical attosecond magnetic fields in the molecular ion H_2^+ using few-cycle circularly polarized attosecond UV pulses by creating time-dependent electron ring currents in the continuum. Comparing with those previous processes in aromatic molecules where the electric currents are created by stationary state electron currents of π orbitals [18–20], one sees that generation of the attosecond-magnetic-field pulses from free electron currents can be readily controlled to yield magnetic fields $\mathbf{B}(t)$ which are a function of velocities $\mathbf{v}$ and displacements $\mathbf{r}$ of ionized electrons, in Eq. (9). These are determined by frequency and duration of circularly polarized attosecond pulses [23]. Using a circularly polarized attosecond pulse with proper conditions, strong magnetic-field pulses with several tens of Teslas can be produced. The radii of the free electron is critically sensitive to the pulse wavelength as defined by the classical model [Eq. (7)]. As a result altering the pulse wavelength leads to an increase or decrease of the efficiency of the attosecond-magnetic-field-pulse generation. Such a scheme to generate attosecond-magnetic-field pulses can also be extended to complex molecular systems with many nuclear centers and multiple electrons. In the latter case, inner shell ionization must be considered [32]. Of note is that interference effects of multiple electronic currents will influence the attosecond-magnetic-field-pulse generation. These magnetic-field pulses should be useful for studying molecular paramagnetic bonding [33], nonequilibrium electronic processes [34], demagnetization processes [35], and optical magnetic recording [14], thus offering experimentalists new tools for controlling electron dynamics on an attosecond time scale.

[1] P. B. Corkum and F. Krausz, Nat. Phys. **3**, 381 (2007).

[2] F. Krausz and M. Ivanov, Rev. Mod. Phys. **81**, 163 (2009).

[3] Z. Chang and P. Corkum, J. Opt. Soc. Am. B **27**, B9 (2010).

[4] K. Zhao, Q. Zhang, M. Chini, Y. Wu, X. Wang, and Z. Chang, Opt. Lett. **37**, 3891 (2012).

[5] T. Popmintchev *et al.*, Science **336**, 1287 (2012).

[6] S. Chelkowski, G. L. Yudin, and A. D. Bandrauk, J. Phys. B **39**, S409 (2006).

[7] H. Niikura, D. M. Villeneuve, and P. B. Corkum, Phys. Rev. Lett. **94**, 083003 (2005).

[8] H. C. Shao and A. F. Starace, Phys. Rev. Lett. **105**, 263201 (2010).

[9] M. J. J. Vrakking and T. E. Elsaesser, Nat. Photon. **6**, 645 (2012).

[10] J. Mauritsson *et al.*, Phys. Rev. Lett. **105**, 053001 (2010).

[11] T. Bredtmann, S. Chelkowski, and A. D. Bandrauk, Phys. Rev. A **84**, 021401 (2011); S. Chelkowski, T. Bredtmann, and A. D. Bandrauk, *ibid.* **85**, 033404 (2012).

[12] X. Wang and J. H. Eberly, Phys. Rev. Lett. **103**, 103007 (2009); **105**, 083001 (2010).

[13] F. Mauger, C. Chandre, and T. Uzer, Phys. Rev. Lett. **104**, 043005 (2010); **105**, 083002 (2010).

[14] C. D. Stanciu, F. Hansteen, A. V. Kimel, A. Kirilyuk, A. T. Tsukamoto, A. Itoh, and Th. Rasing, Phys. Rev. Lett. **99**, 047601 (2007).

[15] C. H. R. Ooi, W. L. Ho, and A. D. Bandrauk, Phys. Rev. A **86**, 023410 (2012).

[16] K. J. Yuan and A. D. Bandrauk, Phys. Rev. Lett. **110**, 023003 (2013).

[17] J. P. van der Ziel, P. S. Pershan, and L. D. Malmstrom, Phys. Rev. Lett. **15**, 190 (1965).

[18] P. S. Pershan, J. P. van der Ziel, and L. D. Malmstrom, Phys. Rev. **143**, 574 (1966).

[19] M. Kanno, H. Kono, Y. Fujimura, and S. H. Lin, Phys. Rev. Lett. **104**, 108302 (2010).

[20] I. Barth, J. Manz, Y. Shigeta, and K. Yagi, J. Am. Chem. Soc. **128**, 7043 (2006); I. Barth and J. Manz, Phys. Rev. A **75**, 012510 (2007).

[21] I. Barth, L. Serrano-Andrés, and T. Seideman, J. Chem. Phys. **129**, 164303 (2008).

[22] K. Nobusada and K. Yabana, Phys. Rev. A **75**, 032518 (2007).

[23] E. Rasanen, A. Castro, J. Werschnik, A. Rubio, and E. K. U. Gross, Phys. Rev. Lett. **98**, 157404 (2007).

[24] K. J. Yuan and A. D. Bandrauk, J. Phys. B **45**, 074001 (2012).

[25] K. F. Lee, D. M. Villeneuve, P. B. Corkum, A. Stolow, and J. G. Underwood, Phys. Rev. Lett. **97**, 173001 (2006).

[26] A. D. Bandrauk and H. Shen, J. Chem. Phys. **99**, 1185 (1993).

[27] A. D. Bandrauk and H. Z. Lu, in *High-Dimensional Partial Differential Equations in Science and Engineering*, edited by A. D. Bandrauk, M. Delfour, and C. LeBris, CRM Lecture Series Vol. 41 (American Mathematical Society, Philadelphia, 2007), pp. 1–15.

[28] O. D. Jefimenko, *Electricity and Magnetism: An Introduction to the Theory of Electric and Magnetic Fields*, 2nd ed. (Electret Scientific Co., Star City, West Virginia, 1989); Am. J. Phys. **58**, 505 (1990).

[29] K. J. Yuan and A. D. Bandrauk, J. Phys. B **45**, 105601 (2012).

[30] P. B. Corkum, N. H. Burnett, and F. Brunel, Phys. Rev. Lett. **62**, 1259 (1989).

[31] P. B. Corkum, Phys. Rev. Lett. **71**, 1994 (1993).

[32] A. Talebpour, A. D. Bandrauk, J. Yang, and S. L. Chin, Chem. Phys. Lett. **313**, 789 (1999); A. Talebpour, A. D. Bandrauk, and S. L. Chin, Laser Phys. **10**, 210 (2000).

[33] K. K. Lange, E. I. Tellgren, M. R. Hoffmann, and T. Helgaker, Science **337**, 327 (2012).

[34] A. Matos-Abiague and J. Berakdar, Phys. Rev. Lett. **94**, 166801 (2005).

[35] C. La-O-Vorakiat *et al.*, Phys. Rev. X **2**, 011005 (2012).